Renewable and Sustainable Energy Reviews 14 (2010) 1969–1978

Contents lists available at ScienceDirect

Renewable and Sustainable Energy Reviews

journal homepage: www.elsevier.com/locate/rser

A simulation study of performance evaluation of single-stage absorption refrigeration system using conventional working fluids and alternatives

M.I. Karamangil [a], S. Coskun [b], O. Kaynakli [a,*], N. Yamankaradeniz [b]

[a] University of Uludag, Faculty of Engineering and Architecture, Department of Automotive Engineering, 16059 Bursa, Turkey
[b] University of Uludag, Vocational School of Technical Sciences, Air Conditioning and Refrigeration Program, 16059, Bursa, Turkey

ARTICLE INFO

Article history:
Received 16 March 2010
Accepted 14 April 2010

Keywords:
Absorption refrigeration
Simulation
Heat exchangers
Solutions
Alternative solutions

ABSTRACT

This study presents a literature review, especially in recent years, on the absorption refrigeration systems (*ARSs*), the currently used refrigerant–absorbent pairs and their alternatives. Additionally, in this study, the thermodynamic analysis of *ARS* using commonly encountered solution pairs in the literature was carried out, and a user-friendly software package including visual components was developed. The effects of operating temperatures, the effectivenesses of solution, refrigerant and solution–refrigerant heat exchangers (*SHE*, *RHE*, *SRHE*), and selection of working fluid pair on the system performance were examined by using the developed package. It was concluded that performances of the cycles improve with increasing generator and evaporator temperatures, but reduce with increasing condenser and absorber temperatures. The performance of system was affected from the *SHE* more than the *RHE* and *SRHE*. While the use of *SHE* improves the system *COP* up to 66%, *RHE* and *SRHE* have an effect of only 14% and 6%, respectively. For that reason, the *SRHE* may not be considered practically significant. Suitable solutions depending on operating conditions showed variations with respect to generator and evaporator temperatures.

Contents

1. Introduction

Vapor compression systems have been used in many refrigeration and air-conditioning applications. However, increased global warming and environmental effect of chlorofluorocarbon has stimulated interest in the development of absorption systems. As the millennium approaches, research on efficient and 'environmentally friendly' technologies is becoming a high priority. Absorption refrigeration systems (*ARSs*) are attractive because they can employ natural refrigerants (water, ammonia, methanol, etc.), and can be driven by waste heat, solar or geothermal energy, and hence support to reduce the fossil fuel consumption. For this reason, the absorption systems are seen as one of the convenient ways of reducing the emissions of greenhouse gasses such as CO_2 [1–3].

Absorption refrigeration system uses various refrigerant–absorbent combinations known as the solution pairs. The absorbent acts as a secondary fluid to absorb the primary fluid which is the refrigerant in its vapor phase. The most widely used working fluid pairs in *ARSs* have been ammonia–water (NH_3–H_2O) and water–lithium bromide (H_2O–LiBr) solutions. The NH_3–H_2O *ARS* is generally used in large capacity industrial applications requiring low temperatures for process cooling. However, H_2O–LiBr

* Corresponding author at: University of Uludag, Faculty of Engineering and Architecture, Department of Automotive Engineering, 16059, Bursa, Turkey. Tel.: +90 224 2941984; fax: +90 224 2941903.
E-mail address: kaynakli@uludag.edu.tr (O. Kaynakli).

1364-0321/$ – see front matter © 2010 Elsevier Ltd. All rights reserved.
doi:10.1016/j.rser.2010.04.008

Nomenclature

COP	coefficient of performance
FR	flow ratio
h	enthalpy (kJ/kg)
$\dot{m}$	mass flow rate (kg/s)
p	pressure (kPa)
q	heat capacity (kJ/kg)
RHE	refrigerant heat exchanger
SHE	solution heat exchanger
SRHE	solution–refrigerant heat exchanger
T	temperature (°C)
ARS	absorption refrigeration system
v	specific volume (m^3/kg)
w	pump work (kJ/kg)
X	solution concentration
ε	effectiveness of heat exchanger
η	isentropic efficiency of pump

Subscripts

a	actual process
A	absorber
c	Carnot
C	condenser
E	evaporator
G	generator
P	pump
s	isentropic process
SS	strong solution
WS	weak solution
1–14	state points

systems are used where moderate temperatures are required (e.g. air-conditioning and chilling applications) and the system is more efficient than the former one. Efforts are being made to search for better refrigerant–absorbent pairs to improve the system performance.

In the absorption refrigeration cycles, it is very important to select the appropriate working substance, the properties of which have a great effect on the performance of the cycles. In recent years, a great many studies have focused on this problem. Ajib and Karno [4] presented the thermal physical properties of acetone–zinc bromide (acetone–$ZnBr_2$) solution for absorption refrigeration systems at low-drive temperatures (about 55 °C). In this pair, acetone is used as coolant and advantages of the solution are based on the needed low temperature heat sources. Theoretical and experimental investigation of absorption refrigeration system using the acetone–$ZnBr_2$ solution was carried out by Karno and Ajib [5]. As a result, they informed that the system can be operated at 50 °C generator temperature without problems and thus, it can be considered as a suitable solution for solar applications. They found that the *COP* was achieved as 0.4 (by measuring) and 0.6 (by simulation). Pilatowsky et al. [6] suggested the new solution monomethylamine–water (CH_3NH_2–H_2O) at low temperatures of 60–80 °C. The performance characteristic of the absorption refrigeration system with this new working solution were analyzed theoretically, the *COP* varied from 0.05 to 0.55 at generator temperature of 60 °C and evaporator temperatures from −5 to 10 °C. According to the study, however, the disadvantage of the solution is that the *COP* was low and a rectification for the vapor produced in the generator was required. Then Pilatowsky et al. [7] investigated the solar absorption refrigeration system working this solution, and suggested that CH_3NH_2–H_2O is a good candidate for the systems operating at evaporator temperatures of −5 to 10 °C. Also Romero et al. [8] studied on the CH_3NH_2–H_2O working pair. In that study, the equations for thermodynamic properties (pressure, concentration, temperature and enthalpy) were expressed in polynomial form. Also it was found that since the CH_3NH_2–H_2O solution have high values of *COP* for the generator temperatures between 60 and 83 °C, it can be used in low enthalpy sources such as solar energy and industrial waste heat. Mittal et al. [9] presented a modeling of solar absorption refrigeration system using H_2O–LiBr. In that study, the certain data (geographical, weather) of Bahal, India was used for falling solar radiation. De Lucas et al. [10] suggested the absorbent (lithium bromide + potassium formate [LiBr + CHO_2K]) instead of the pure LiBr for the refrigerant (H_2O) to lower the required drive temperature. The authors' more recent study, De Lucas et al. [11] stated on the effect of the addition of a surfactant (*n*-octanol) on the solutions to improve the absorption capacity. Riffat et al. [2] experimentally studied on the absorption and desorption characteristics of a water–potassium formate (H_2O–CHO_2K) and water–lithium bromide (H_2O–LiBr) binary mixtures. As a result, the desorption rates of H_2O–CHO_2K was found to be higher than that of H_2O–LiBr. They emphasized that the increase in desorption rate would decrease the energy required in the generator and so improve the efficiency of absorption cycle. Moreover, in that study, it was indicated that the physical properties of H_2O–CHO_2K are more attractive than those of H_2O–LiBr since it is less in cost of production, less corrosive, and more ecologically acceptable. Thermodynamic and physical properties for the ammonia–lithium nitrate (NH_3–$LiNO_3$) and ammonia–sodium thiocyanate (NH_3–NaSCN) solutions were presented by Ferreira [12], and interesting comparisons between NH_3–H_2O, NH_3–$LiNO_3$ and NH_3–NaSCN absorption systems may be found in Sun [13] and Abdulateef et al. [14]. Among ammonia-based mixtures, although the NH_3–NaSCN can be considered as an alternative solution to H_2O–NH_3, Sun [13] emphasized that this solution cannot be operated at evaporator temperatures below −10 °C for the possibility of crystallization. One of the more recent studies, Zhu and Gu [15] performed a theoretical analysis of the absorption refrigeration cycle using NH_3–NaSCN solution, where the NaSCN is used as the absorbent and the NH_3 is used as the refrigerant. They found that the solution is advantageous for lower generator temperatures compare to NH_3–H_2O solution, because of the fact that the *COP* is about 10% higher than the ones for NH_3–H_2O system at the same working conditions. Safarov [16] presented the properties of methanol–lithium bromide (CH_3OH–LiBr) solution, the viscosity of which is lower than H_2O–LiBr solution, and the use of the solution provides an opportunity for the temperatures below the freezing point of water. And then Safarov [17] presented the experimental vapor pressures of CH_3OH–LiBr and methanol–lithium chloride (CH_3OH–LiCl) solutions at 298.15–323.15 K. Sencan [18] used a number of methods, which are linear regression, pace regression, sequential minimal optimization, M5 model tree, M5'Rules and back propagation neural network (BPNN), in order to determine the specific volume of CH_3OH–LiBr and CH_3OH–LiCl fluid couples. In that study, among these methods BPNN method was recommended to be most accurate and quick (R^2 value is 0.9840 for CH_3OH–LiBr, 0.996 for CH_3OH–LiCl).

Muthu et al. [19] emphasized the limitations of H_2O–LiBr solution, which are as follows: the evaporator temperature is limited to about 5 °C as water is used as a refrigerant, the system is operated under very low (high vacuum) pressures, and there is also possibility of crystallization (solidification) of the lithium bromide solution; and the limitations of NH_3–H_2O solution, which are as follows: this system is toxic, rectification is necessary, copper cannot be used due to corrosion problem, and ammonia with air is

flammable when its concentration is about 25% by volume. Because of these reasons, they experimentally analyzed the R134a-dimethyl acetamide (DMAC) absorption refrigeration system. At the evaporating temperature of 7 °C, the theoretical and actual *COP*s were obtained as 0.50 and 0.45, respectively, for the sink and heat source temperatures of 20 and 65 °C. They found that the R134a-DMAC can be used as a working fluid in absorption refrigerators using low potential heat sources. Kaita [20] developed the equations giving the thermodynamic properties of H_2O–LiBr solution for high temperatures from 40 to 210 °C, and also for concentrations of 40–65%. These equations could be used in triple-effect H_2O–LiBr chillers. In Chua et al. [21], a thermodynamically consistent set of specific enthalpy, entropy, and heat capacity fields for the LiBr–H_2O solution was derived for the temperature range from 0 to 190 °C, and the concentration range from 0 to 75%. Wu and Eames [22] reviewed some innovations in vapor absorption technology, and stated on the cycle designs and working fluid selection. As a consequence, they emphasized that although much of effort has been made to find and improve the working fluids for absorption systems, H_2O–LiBr and NH_3–H_2O pairs are still the best in general use.

The variations of various performance parameters of *ARS* were compared for water-based 16 different mixtures in Saravanan and Maiya [23]. They concluded that the H_2O–LiBr + LiCl + $ZnCl_2$ combination showed the better *COP*. Mostafavi and Agnew [24,25] investigated the effect of ambient temperature on the component geometry and the performance of the *ARS* using H_2O–LiBr. Horuz [26] carried out an investigation to analyze the *ARS*s using NH_3–H_2O and H_2O–LiBr solutions and compared them in respect of the performances, cooling capacity and the maximum and minimum system pressures. Bulgan [27] investigated the use of low temperature energy sources, especially in the range of 85–110 °C, in the *ARS* using ammonia–water. The effects of important design and working parameters on performance of the system were obtained. In that study, the variation of system *COP* and circulation ratio values were examined for different source temperatures. The thermodynamic properties of CH_3OH–LiBr and CH_3OH–LiCl solutions in the ranges of 0.1–40 MPa, 298–498 K, 2–12% were experimentally investigated and presented in the study of Bulgan et al. [28]. Joudi and Lafta [29] carried out a steady-state simulation model based on heat and mass balance equations as well as fluid flow, heat, and mass transfer correlations. Simultaneous heat and mass transfer were considered in the absorber instead of heat transfer alone. Aphornratana and Sriveerakul [30] experimentally investigated the system performance of single-effect absorption refrigerator using H_2O–LiBr. The actual (experimental) *COP* was found to be approximately 80% of the theoretical *COP*. They emphasized that the difference was due to low mass transfer performance of the absorber, and if a more effective absorber was used, the actual *COP* as high as the theoretical one should be achieved. Moreover, they found that the generator energy input could be reduced by up to 60% by using a solution heat exchanger resulting in a greater *COP*, and the H_2O–LiBr system could be operated at low generator temperatures (about 65 °C) and it still maintains the performance. Mehrabian and Shahbeik [31] developed a computer program for thermodynamic analysis of single-effect *ARS* using H_2O–LiBr solution. In that study, the thermodynamic properties of all state points were given and the effect of solution heat exchanger effectiveness on the *COP* was investigated by using the developed computer program. However, the program does not include other currently used solutions such as ammonia-based mixtures, and other heat exchangers such as *RHE* and *SRHE*.

One of the good literature reviews about absorption refrigeration technologies is the study of Srikhirin et al. [32] where a number of research options such as possible operating configurations of absorption refrigeration cycles, research on working fluids, and improvement of absorption processes were discussed. A more recent review study was presented by Zhai and Wang [33] for solar sorption (absorption and adsorption) refrigeration systems in China. Also a similar review for sorption refrigeration systems was carried out, and application areas of these technologies were categorized by Fan et al. [34]. They emphasized that these systems are attractive technologies that not only can serve the needs for refrigeration, air-conditioning and ice making applications, but also can meet demand for energy conservation and environment protection. Furthermore, comparatively, absorption systems are more suitable for air-conditioning while adsorption systems are more employed for low temperature purpose.

Relatively few studies have, on the other hand, been focused on the only absorbent instead of solution pairs used in *ARS*s such as De Lucas et al. [10] and Donate et al. [35]. Mixtures of lithium bromide and the four organic salts (potassium formate, sodium formate, potassium acetate and sodium lactate) were evaluated as alternative absorbents for absorption refrigeration systems in Donate et al. [35].

Many studies dealt with the thermodynamic analysis and performance evaluation of absorption refrigeration systems. Among these studies, Sozen and Ozalp [36] studied on absorption refrigeration system working with NH_3–H_2O in order to achieve better performance. For this purpose, the ejector was located at the absorber inlet. As a result, they found that the *COP* was improved by 49% and the circulation ratio was reduced by 57%. Abu-Ein et al. [37] presented the theoretical analysis of solar powered absorption refrigeration system using NH_3–H_2O solution. The minimum and maximum *COP* values were obtained at generator temperatures of 110 and 200 °C for all evaporator temperatures. A detailed thermodynamic analysis of H_2O–LiBr absorption refrigeration cycle was performed in the study of Kaynakli and Kilic [38]. The influences of operating temperature and effectivenesses of heat exchangers (*SHE* and *RHE*) on the thermal loads of components, coefficients of performance (COP_c, *COP*) and efficiency ratio were investigated. Sencan [39] applied the artificial neural network model to determine the *COP* of single-stage absorption refrigeration system using NH_3–H_2O solution. This study emphasized that the new methodology provides faster and simpler solutions instead of complex functions based on analytic equations used for calculating the properties of fluids or refrigerant–absorbent pairs. Similarly Sozen et al. [40] used the artificial neural network approach for the formulation of thermodynamic properties of the refrigerant–absorbent pairs, which are methanol–LiBr and methanol–LiCl. Misra et al. [41] used the average cost approach to optimize H_2O–LiBr absorption refrigeration system. This method consists of exergy analysis followed by the determination of the average cost per unit exergy of all internal flows and products appearing in the thermoeconomic representation of the system. Experimental analysis of the performance of an absorption refrigerator using H_2O–LiBr binary mixture under different service conditions were carried out by Asdrubali and Grignaffini [42]. They found that the absorption machine shows the highest values of *COP* at temperatures around 70 °C, thus making it possible to work this machine with solar collectors. A commercial absorption refrigeration water–ammonia chiller made by Robur was experimentally tested by Horuz and Callander [43]. Then, Robur absorption refrigeration chiller was analyzed using Aspen Plus flowsheet simulator, which has databases for the physical–chemical properties of chemical substances, in the study of Darwish et al. [44]. The predicted results of various performance parameters were compared with the experimental and some manufacturer data reported in the literature on the same unit. They concluded that overall, the agreement is very good and the validity of the use of Aspen Plus simulator in performance analyses of thermodynamic cycles is evident. Venegas et al. [45] simulated the use of low

temperature heat (between 50 and 90 °C) in double- and triple-stage absorption refrigeration and heat pump systems using NH_3–H_2O, NH_3–$LiNO_3$ and NH_3–NaSCN solutions. In general, the refrigeration and heat pump cycles reached higher *COP* values using an NH_3–$LiNO_3$ solution. Wang et al. [46] dealt with an improved absorption refrigeration cycle using NH_3–$LiNO_3$ with staged absorption. The improved cycle used a series of absorbers among which one was cooled by the external medium and the others were cooled by refrigerant at staged pressures between the evaporation and condensation pressures. The simulation results in that study demonstrated that the improved cycle was able to steadily run when driven by low-grade thermal sources as low as 65 °C, and to produce deep refrigeration temperature as low as −40 °C. On the other hand, diffusion absorption refrigeration systems were examined by Zohar et al. [47–49] and Koyfman et al. [50].

To improve the performance, some researchers studied the cascade refrigeration systems [51–54]. Fernandez-Seara et al. [51] investigated a refrigeration system in cascade with a compression system using CO_2 at the low temperature stage and an absorption system using NH_3–H_2O solution at the higher temperature stage to generate cooling at low temperatures and in addition to this, to reduce the energy consumption. He and Chen [53] and He et al. [54] used the mixtures of R32 and R134a as refrigerant, the dimethylformamide (DMF) as absorbent in a cascade absorption refrigeration system to obtain low refrigerating temperatures as low as −50 °C. This refrigeration temperature is much lower than that obtained by traditional absorption refrigeration cycle. According to these studies, the new cycle, theoretically, could achieve −62 °C refrigeration temperature when the generation temperature was 160 °C, on the other hand, −47.3 °C refrigeration temperature was achieved by experiment at the generation temperature of 157 °C.

Heat is wasted to the environment in most applications, such as exhaust gas from vehicles. Manzela et al. [55] and Koehler et al. [56] researched the feasibility and potential of using the internal combustion engine exhaust gas as an energy source for absorption refrigeration systems. Manzela et al. [55] also investigated its influence on the engine performance. Hilali and Soylemez [57] optimized the size of generator in which waste heat recovery occurs. P_1–P_2 method was used and concluded that the optimum effectiveness was found as 0.751 and the optimum heat transfer area was found as 1.07 m^2. Sun and Guo [58] tested a prototype of combined compression–absorption refrigeration system, waste heat from gas engine (the temperature of the exhaust gas was 120 °C) was used to operate single-effect absorption refrigeration cycle. Exhaust gas was recovered by a shell–tube heat exchanger. The experimental results showed that the combined refrigeration system was feasible because of the fact that the prototype system saved about 25% of primary energy compared to a conventional electrically driven vapor compression refrigeration unit.

In this study, firstly we present a literature review on the absorption refrigeration systems using different refrigerant–absorbent pairs, and the system performances. The review concentrates on literature produced especially over the last decade. And then, a visual software package for simulating the performances of absorption refrigeration systems working on different solution pairs is developed by Delphi programming language. It is hoped that the developed user-friendly software package would serve the selection of appropriate working solution pair in the absorption refrigeration system, the accurate and fast calculation of performance parameters, the determination of suitable operating conditions.

2. Mathematical model

2.1. Thermodynamic analysis of ARS

The schematic illustration of the single-stage *ARS* is presented in Fig. 1. As this figure illustrates, the *ARS* contains a generator, an absorber, a condenser, an evaporator, a pump, an expansion valve, a solution heat exchanger (*SHE*), a refrigerant heat exchanger (*RHE*, precooler) and a solution–refrigerant heat exchanger (*SRHE*). When the refrigerant leaves the evaporator, it is not mechanically compressed, but it is absorbed by a second working fluid. The liquid mixture of absorbent and refrigerant is pumped to a higher pressure and into the generator. The pumping process is driven by a work input, but the amount of work that is required is an order of magnitude less than it is a vapor compression cycle. Direct thermal energy from a high-temperature source is transferred to the refrigerant–absorbent mixture in the generator. This heating

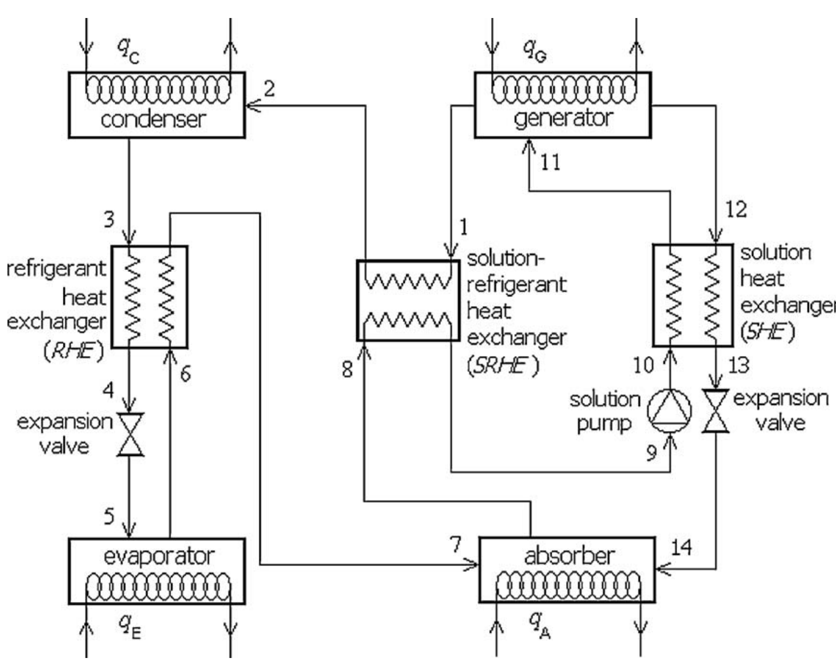


Fig. 1. The schematic illustration of the single-stage *ARS*.

process generates refrigerant vapor, which flows into the condenser. The remaining liquid absorbent is then throttled back to the lower system pressure as it falls from the generator into the absorber.

Mass balance at the generator can be written as follows:

- For H_2O–LiBr:

$$\dot{m}_{WS} = \dot{m}_{SS} + \dot{m}_{H_2O} \quad \text{(total mass balance)} \tag{1}$$

$$\dot{m}_{WS}X_{WS} = \dot{m}_{SS}X_{SS} \quad \text{(LiBr balance)} \tag{2}$$

- For ammonia-based mixtures:

$$\dot{m}_{SS} = \dot{m}_{WS} + \dot{m}_{NH_3} \quad \text{(total mass balance)} \tag{3}$$

$$\dot{m}_{SS}X_{SS} = \dot{m}_{WS}X_{WS} + \dot{m}_{NH_3} \quad \text{(ammonia balance)} \tag{4}$$

From Eqs. (1)–(4), the strong and weak solution mass flow rates can be determined as follows:

- For H_2O–LiBr:

$$\dot{m}_{SS} = \frac{X_{WS}}{X_{SS} - X_{WS}}\dot{m}_{H_2O} \tag{5}$$

$$\dot{m}_{WS} = \frac{X_{SS}}{X_{SS} - X_{WS}}\dot{m}_{H_2O} \tag{6}$$

- For ammonia-based mixtures:

$$\dot{m}_{SS} = \frac{1 - X_{WS}}{X_{SS} - X_{WS}}\dot{m}_{NH_3} \tag{7}$$

$$\dot{m}_{WS} = \frac{1 - X_{SS}}{X_{SS} - X_{WS}}\dot{m}_{NH_3} \tag{8}$$

The flow ratio (*FR*) can be defined as the ratio of the mass flow rate of the solution through the pump to the mass flow rate of the working fluid. One of the importances of the *FR* should be noted as it represents the required pumping energy. On the other hand, if it is higher than that expected, the performance of absorber can be adversely affected [30].

- For H_2O–LiBr:

$$FR = \frac{\dot{m}_{WS}}{\dot{m}_{H_2O}} = \frac{X_{SS}}{X_{SS} - X_{WS}} \tag{9}$$

- For ammonia-based mixtures:

$$FR = \frac{\dot{m}_{SS}}{\dot{m}_{NH_3}} = \frac{1 - X_{WS}}{X_{SS} - X_{WS}} \tag{10}$$

The heat capacities of the main components of the *ARS* can be calculated as follows:

$$q_E = h_6 - h_5 \tag{11}$$

$$q_C = h_2 - h_3 \tag{12}$$

$$q_G = h_1 + (FR - 1)h_{11} - FR\,h_{12} \tag{13}$$

$$q_A = FR\,h_8 - (FR - 1)h_{14} - h_7 \tag{14}$$

The energy balance and heat capacity equations of the solution heat exchanger are given by:

$$T_{13} = \varepsilon_{SHE}T_{10} + (1 - \varepsilon_{SHE})T_{12} \tag{15}$$

$$h_{11} = h_{10} + (h_{12} - h_{13})\frac{FR - 1}{FR} \tag{16}$$

$$q_{SHE} = (h_{12} - h_{13})(FR - 1) = (h_{11} - h_{10})FR \tag{17}$$

The saturated liquid from the condenser and the saturated vapor from the evaporator enter the refrigerant heat exchanger, oriented at the refrigeration side. The saturated vapor receives heat and leaves the *RHE* as superheated vapor while saturated liquid gives heat and leaves as sub-cooled liquid. Then the energy balance for the *RHE* is written as:

$$h_7 = h_6 + \varepsilon_{RHE}(h_{7(T3)} - h_6) \tag{18}$$

$$h_4 = h_3 - \varepsilon_{RHE}(h_{7(T3)} - h_6) \tag{19}$$

where $h_{7(T3)}$ is the enthalpy of superheated vapor at the condenser temperature. The heat capacity of the *RHE* per unit refrigerant mass flow rate can be calculated as:

$$q_{RHE} = h_3 - h_4 = h_7 - h_6 \tag{20}$$

The energy balance for solution–refrigerant heat exchanger can be written as:

$$h_2 = h_1 - \varepsilon_{SRHE}(h_1 - h_{2(T8)}) \tag{21}$$

$$h_9 = h_8 + (h_1 - h_{2(T8)})\frac{\varepsilon_{SRHE}}{FR} \tag{22}$$

where $h_{2(T8)}$ is the enthalpy of vapor at absorber temperature. The heat capacity of the *SRHE* per unit refrigerant mass flow rate can be calculated as:

$$q_{SRHE} = h_1 - h_2 = (h_9 - h_8)FR \tag{23}$$

Pump work per unit refrigerant mass flow rate can be determined as follows:

$$w_P = FR(p_C - p_E)\frac{v}{\eta_P} \tag{24}$$

where η_P is the isentropic efficiency of a pump. When the changes in potential and kinetic energies of a liquid are negligible, the η_P is defined as:

$$\eta_P = \frac{w_s}{w_a} = \frac{h_{10,s} - h_9}{h_{10,a} - h_9} \tag{25}$$

where $h_{10,a}$ and $h_{10,s}$ are the enthalpies at the exit for actual and isentropic process, respectively. The enthalpy at the solution pump outlet can be determined as follows:

$$h_{10,a} = h_9 + (p_C - p_E)\frac{v}{\eta_P} \tag{26}$$

The measure of performance of refrigerators is expressed in terms of coefficient of performance (*COP*), defined as:

$$COP = \frac{q_E}{q_G + w_P} \tag{27}$$

2.2. Theoretical calculations in the software package

For a single-stage absorption refrigeration cycle, the theoretical calculations of the *FR* and the *COP* have been performed with the values of temperatures (T_G, T_A, T_C, T_E), heat changer effectivenesses (ε_{SHE}, ε_{RHE}, ε_{SRHE}), pump efficiency (η_P) and assuming the following conditions: (1) The systems are simulated under steady-state conditions. (2) The pressure in the generator, condenser, evaporator and absorber are equal to the vapor pressure of the working fluids. (3) The pressure drop in the pipes and vessels is negligible. (4) The solutions leaving generator and absorber are at the same temperature and concentration as in the generator and absorber, and they are in thermodynamic equilibrium. (5) The expansion process in the expansion device is at constant enthalpy.

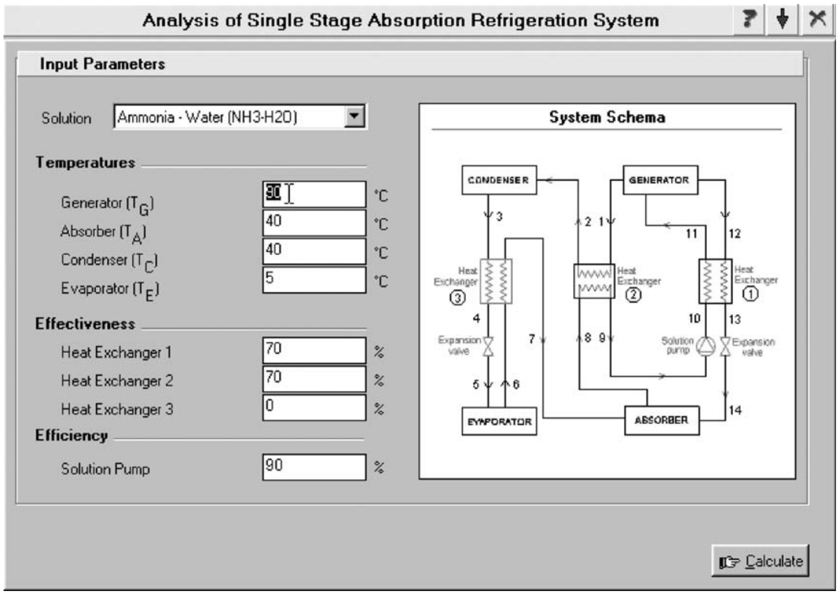


Fig. 2. The Input Page of the visual software package.

2.3. Software program

The developed software package includes screens as follows: the Input Page where the operating conditions are entered, the Output Page-1 where simulation results (the performance parameters and heat transfer rates) are shown, the Output Page-2 where the simulation results for the thermodynamic properties of solutions at each state point of cycle are shown. As an example, the Input Page is shown in Fig. 2. The flow chart of the software program is presented in Fig. 3.

3. Simulation results and discussion

The influence of the effectivenesses of the heat exchangers (*SHE*, *SRHE* and *RHE*) on the performance of system using NH_3–H_2O are shown in Fig. 4. In these simulations, $T_G = 90\,^{\circ}C$, $T_C = T_A = 40\,^{\circ}C$, $T_E = 10\,^{\circ}C$, and $\eta_P = 0.90$ were assumed. Fig. 4 shows that the performance of the system is improved with an increase in the effectivenesses. The effectiveness value having zero means that no heat exchanger is included in the cycle. At this operating conditions, the *COP* value is only 0.39. With the heat exchanger effectivenesses

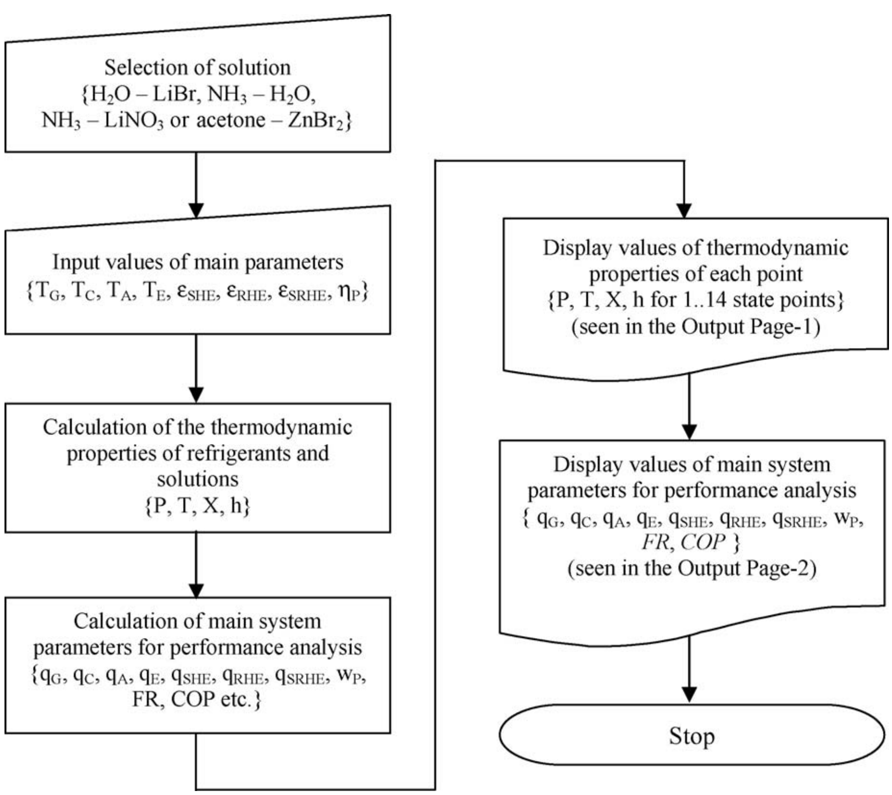


Fig. 3. Flow chart of the simulation.

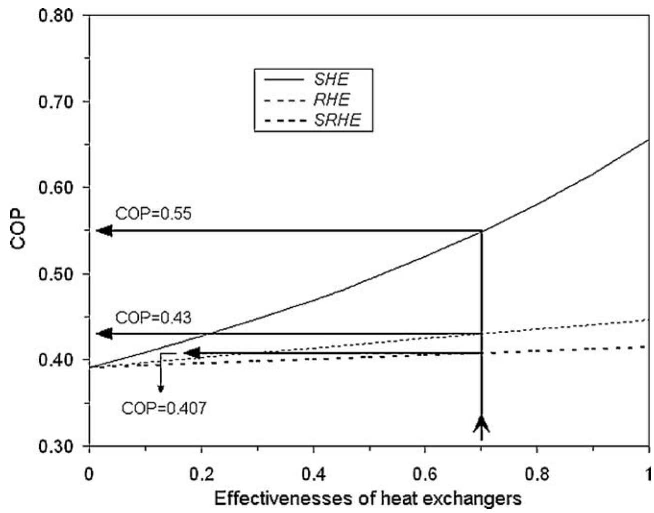


Fig. 4. Variation of *COP* with effectivenesses of heat exchangers.

increase, the system *COP* increases gradually. But, the effect of the *SHE* on the *COP* is more apparent than those of the *SRHE* and *RHE*. As the mass flow rates and the difference between the inlet temperatures of fluids for *SHE* are generally greater than those of other heat exchangers, the amount of heat transfer is higher. With increasing the effectiveness of *SHE*, the energy needed in the generator decreases and thus the system *COP* increases. For the best-case condition of *SHE* ($\varepsilon_{SHE} = 1$, the strong solution outlet temperature equals the weak solution inlet temperature), *COP* value increases up to 0.65 as can be seen in Fig. 4, which is 66% higher than that without *SHE*. This result is in agreement with the studies of Zhu and Gu [15] and Aphornratana and Sriveerakul [30]. Zhu and Gu [15] found that the effect of *SHE* on the increase of *COP* for the *ARS* using NH_3–NaSCN solution was approximately 60%. The effectiveness of heat exchanger can be practically assumed to be 70% [59,60]. It can be observed that for this effectiveness the *COP* value is 0.55, which is 40% higher than that without a solution heat exchanger. On the other hand, it is noted that the heat exchanger effectiveness was assumed as 80% in the theoretical calculations of Sozen [61].

As also seen in Fig. 4, the second-effective heat exchanger is the *RHE*. With increasing the *RHE* effectiveness, the *COP* value increases from 0.39 to 0.45, which indicates 14% improvement in system performance. Since the refrigerant enters the evaporator at a relatively low enthalpy with increasing the effectiveness of *RHE*, the evaporator heat transfer capacity increases and thus the system *COP* rises. On the other hand, the influence of *SRHE* on the *COP* is maximum only 6% (from 0.39 to 0.415). The temperature increase of solution leaving the absorber is small, as the mass flow rate of vapor leaving the generator is relatively small. As can be seen in figure, for the effectiveness of 70%, the *COP* value is 0.407, which is 4% higher than that without *SRHE*. As a result of this, the effect of the *SRHE* on *COP* improvement is practically negligible compared to other heat exchangers. For that reason, in this study, the *SRHE* was not considered in the subsequent analyses.

The effect of operating temperatures on the performance parameters of absorption refrigeration cycle are comparatively presented in Figs. 5–8 for H_2O–LiBr, NH_3–H_2O and NH_3–$LiNO_3$ solutions. *FR* is an important design and optimizing parameter since it is directly related to the size and cost of the generator, absorber, heat exchangers and pump [62]. Because of this, the *FR* values obtained from the simulation are given in figures, together with the *COP* values. When the generator temperature increases, concentration of strong solution of H_2O–LiBr increases and concentration of weak solution of ammonia-based mixtures decreases, hence *FR* decreases as can be seen in Fig. 5. The performance of the systems goes better when the generator temperature increases. Among the solutions the highest

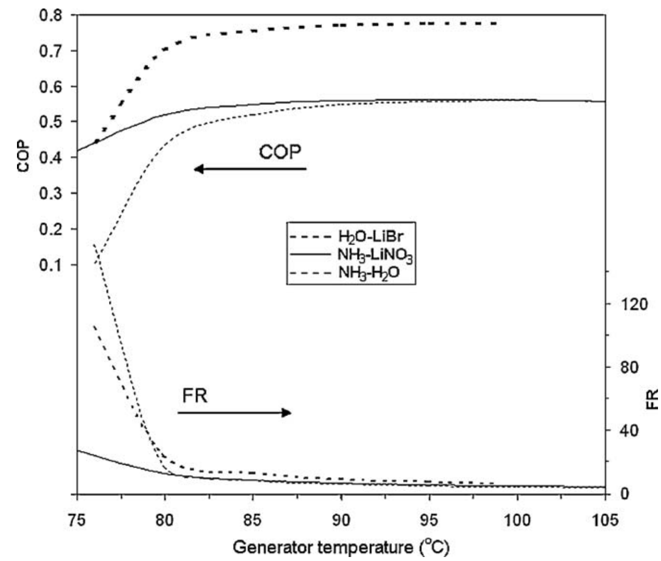


Fig. 5. Variation of *COP* and *FR* with the generator temperature ($T_C = T_A = 40$ °C, $T_E = 5$ °C, $\varepsilon_{SHE} = \varepsilon_{RHE} = 0.70$, $\eta_P = 0.90$).

COP is obtained for H_2O–LiBr solution pair. H_2O–LiBr cycle can operate in a more narrow range of the generator temperatures compared to the systems using ammonia-based mixtures, because of its crystallization possibility. Due to the crystallization problem, the H_2O–LiBr system could not reach above the 100 °C of generator temperature under the given operating conditions. Performances of ammonia-based solutions are quite near to each other for the generator temperature above approximately 90 °C. But especially at low generator temperatures ($T_G < 75$ °C) NH_3–$LiNO_3$ solution has an advantage according to other solutions because of high *COP* values. Variation of *FR* and *COP* values with the evaporator temperature is shown in Fig. 6. *COP* values of the cycles increase on the other hand while *FR* values decrease with increasing evaporator temperature. *COP* values of the ammonia-based solutions are quite near to each other for all evaporator temperatures. As it can be seen in Figs. 5 and 6, the variation of generator temperature strongly affects the *FR*, on the other hand the evaporator temperature variation affects in a less amount. This result agrees with the theoretical results of Sun [13] and

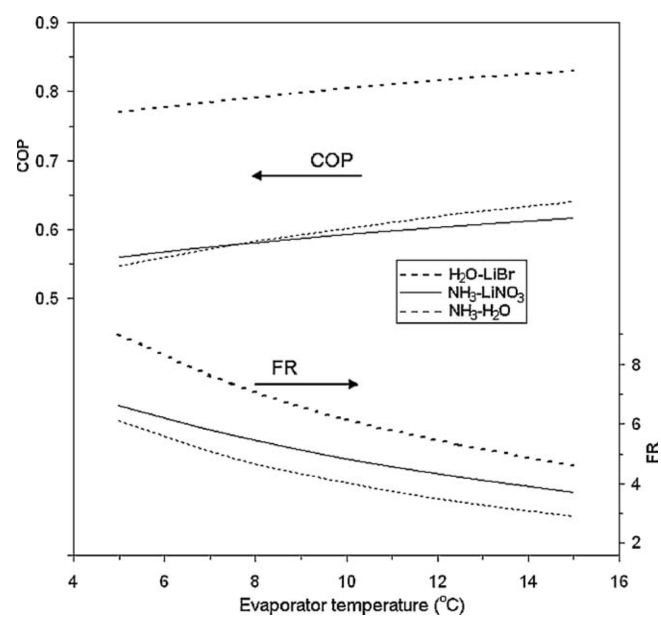


Fig. 6. Variation of *COP* and *FR* with the evaporator temperature ($T_G = 90$ °C, $T_C = T_A = 40$ °C, $\varepsilon_{SHE} = \varepsilon_{RHE} = 0.70$, $\eta_P = 0.90$).

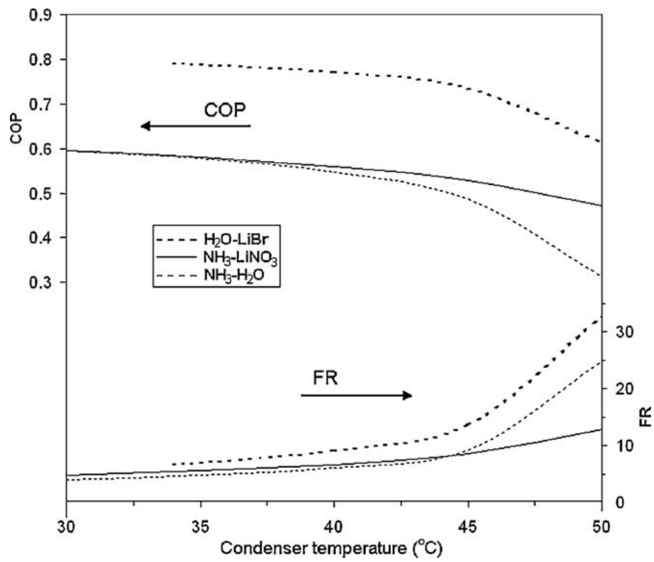


Fig. 7. Variation of *COP* and *FR* with the condenser temperature (T_G = 90 °C, T_A = 40 °C, T_E = 5 °C, $\varepsilon_{SHE} = \varepsilon_{RHE}$ = 0.70, η_P = 0.90).

Saravanan and Maiya [23] and the experimental results of Aphornratana and Sriveerakul [30].

Variation of *FR* and *COP* values with the condenser temperature is given in Fig. 7. When the condenser temperature increases, concentration of strong solution of H_2O–LiBr decreases and concentration of weak solution of ammonia-based mixtures increases, hence *FR* increases. If the condenser temperature increases, *COP* values decrease for all solutions. At the condenser temperature lower than 34 °C, the H_2O–LiBr solution is prone to crystallization. Especially, for the condenser temperatures above 45 °C, *COP* values of H_2O–LiBr and NH_3–H_2O cycles decrease rapidly. Variation of *FR* and *COP* values with the absorber temperature is shown in Fig. 8. The *COP* values of the cycles decrease with increasing of the absorber temperature. The higher *COP* values are obtained for NH_3–$LiNO_3$ solution at the absorber temperatures above 47 °C compared to other solutions. As it can be seen in Figs. 5–8, the *COP* results of NH_3/$LiNO_3$ solution generally show higher values than those of NH_3–H_2O solution for all operating temperatures. This result is in agreement with the studies of Sun [13] and Venegas et al. [45]. Therefore, this solution can be considered as an alternative to NH_3–H_2O pair.

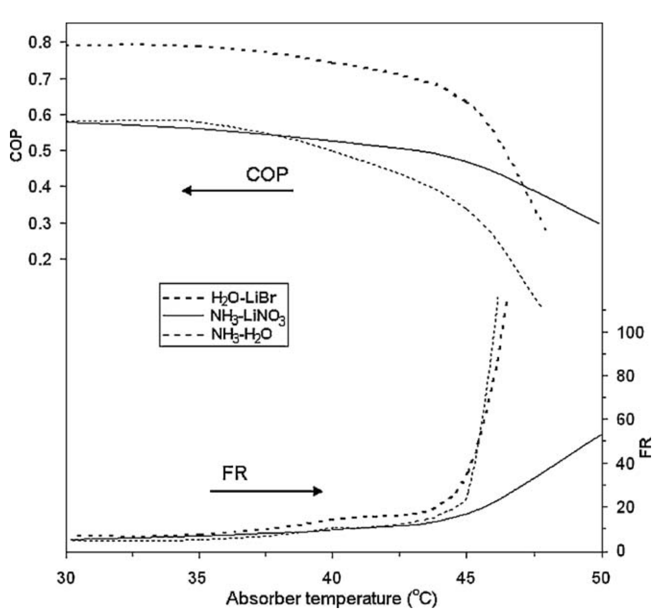


Fig. 8. Variation of *COP* and *FR* with the absorber temperature (T_G = 90 °C, T_C = 40 °C, T_E = 5 °C, $\varepsilon_{SHE} = \varepsilon_{RHE}$ = 0.70, η_P = 0.90).

Table 1
Thermodynamic properties of the solutions.

State points	T (°C)	P (kPa)	X (%)	h (kJ/kg)
H_2O–LiBr cycle				
1	90.00	5.630	0.00	2664.22
2	90.00	5.630	0.00	2664.22
3	35.00	5.630	0.00	146.64
4	26.60	5.630	0.00	111.47
5	4.00	0.812	0.00	111.47
6	4.00	0.812	0.00	2506.73
7	22.50	0.812	0.00	2541.91
8	35.00	0.812	55.83	86.43
9	35.00	0.812	55.83	86.43
10	35.00	5.630	55.83	86.43
11	60.12	5.630	55.83	137.85
12	90.00	5.630	64.59	233.33
13	57.00	5.630	64.59	173.84
14	57.00	0.812	64.59	173.84
NH_3–H_2O cycle				
1	90.00	1349.79	100.00	1636.92
2	90.00	1349.79	100.00	1636.92
3	35.00	1349.79	100.00	343.85
4	25.35	1349.79	100.00	296.90
5	4.00	497.47	100.00	296.90
6	4.00	497.47	100.00	1447.61
7	22.12	497.47	100.00	1494.56
8	35.00	497.47	53.14	−94.17
9	35.00	497.47	53.14	−94.17
10	35.26	1349.79	53.14	−92.98
11	61.64	1349.79	53.14	31.06
12	90.00	1349.79	41.69	160.97
13	57.76	1349.79	41.69	6.61
14	57.76	497.47	41.69	6.61
NH_3–$LiNO_3$ cycle				
1	90.00	1349.79	100.00	1636.92
2	90.00	1349.79	100.00	1636.92
3	35.00	1349.79	100.00	343.85
4	25.35	1349.79	100.00	296.90
5	4.00	497.47	100.00	296.90
6	4.00	497.47	100.00	1447.61
7	22.12	497.47	100.00	1494.56
8	35.00	497.47	53.38	−107.64
9	35.00	497.47	53.38	−107.64
10	35.31	1349.79	53.38	−106.65
11	61.74	1349.79	53.38	−21.86
12	90.00	1349.79	43.76	68.26
13	58.43	1349.79	43.76	−34.02
14	58.43	497.47	43.76	−34.02

In this study, the user-friendly computer program has been developed simulating the performance of single-stage absorption refrigeration system using the solutions which are available in the literature. The simulation results showing the thermodynamic properties of these solutions at each state point of the cycle are given in Table 1. Moreover, the capacity of the components and the *COP* values of the systems are presented in Table 2. In these

Table 2
Components capacities per unit refrigerant mass flow rate and *FR* and *COP* values.

Capacities (kJ/kg)	H_2O–LiBr	NH_3–H_2O	NH_3–$LiNO_3$
Generator (q_G)	3135.0	2137.2	2095.8
Condenser (q_C)	2517.6	1293.1	1293.1
Evaporator (q_E)	2395.3	1150.7	1150.7
Absorber (q_A)	3012.7	2000.9	1959.2
Solution heat exchanger (q_{SHE})	379.2	631.4	496.0
Refrigerant heat exchanger (q_{RHE})	35.2	47.0	47.0
Pump (w_P)	0.02	6.02	5.74
FR	7.37	5.09	5.85
COP	0.76	0.54	0.55

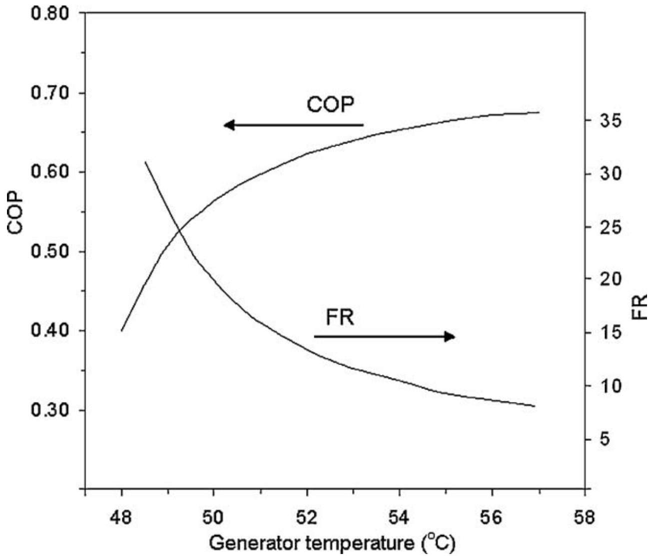


Fig. 9. Variation of *COP* and *FR* with the generator temperature for acetone–$ZnBr_2$ ($T_C = T_A = 28\ ^\circ C$, $T_E = 10\ ^\circ C$, $\varepsilon_{SHE} = \varepsilon_{RHE} = 0.75$, $\eta_P = 0.90$).

calculations $T_G = 90\ ^\circ C$, $T_C = T_A = 35\ ^\circ C$, $T_E = 4\ ^\circ C$, $\varepsilon_{SHE} = \varepsilon_{RHE} = 0.60$ and $\eta_P = 0.90$ were assumed. These results were taken from the Output Page-1 of the developed computer program. The user can easily perform the analyses for different conditions (operating temperatures, effectivenesses of heat exchangers, efficiency of pump, etc.) and see the simulation results in tabular form.

Acetone–zinc bromide (acetone–$ZnBr_2$) solution was analyzed under different operating conditions compared to the above-mentioned solutions since it can be operated at lower generator temperatures. The variation of *COP* and *FR* values of *ARS* using acetone–$ZnBr_2$ with generator and evaporator temperatures are shown in Figs. 9 and 10, respectively. As can be seen from Fig. 9, the *COP* varies between 0.40 and 0.67 for the generator temperatures of 48–57 °C. It can be considered as a suitable solution for low temperature heat sources (about 50–55 °C) such as solar, geothermal or waste heat applications. Moreover, at high evaporator temperatures (above 12 °C) the system *COP* can exceed 0.70 (see Fig. 10). It can be also considered as a suitable solution for air-conditioning applications that require moderate evaporator temperatures since the system *COP* improves with increasing the evaporator temperatures. The *COP* is achieved about 0.70 for the evaporator temperatures of approximately 10 °C. For that reason, it can be evaluated as an alternative to water–lithium bromide solution.

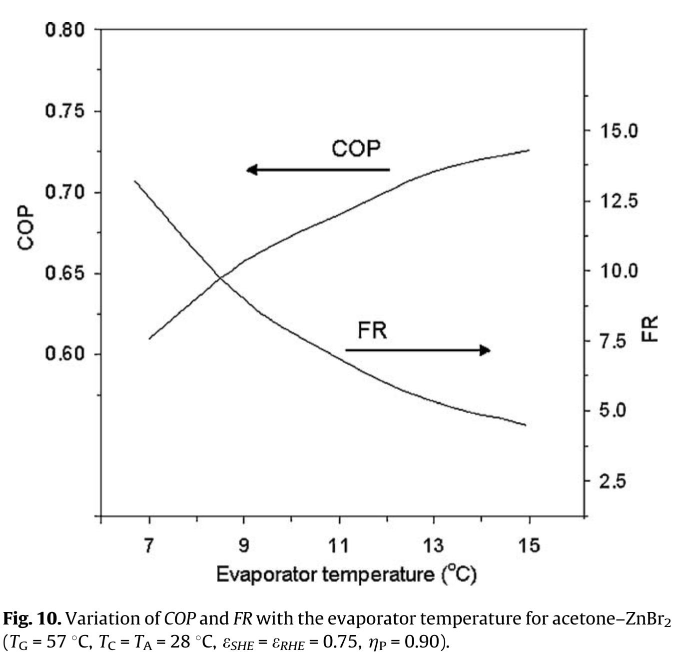


Fig. 10. Variation of *COP* and *FR* with the evaporator temperature for acetone–$ZnBr_2$ ($T_G = 57\ ^\circ C$, $T_C = T_A = 28\ ^\circ C$, $\varepsilon_{SHE} = \varepsilon_{RHE} = 0.75$, $\eta_P = 0.90$).

4. Conclusions

In this study, after a review of the literature on *ARS*s and working fluids was presented, thermodynamic analysis of single-stage *ARS* using different refrigerant–absorbent pairs was performed and the theoretical performances of the cycles were compared. Moreover, a user-friendly visual software package was developed in scope of this study. The simulation results showed that the *COP* values of the cycles increase with increasing generator and evaporator temperatures, but decrease with increasing condenser and absorber temperatures as expected. Furthermore, the generator temperature has a great effect on the *COP* and *FR* values of systems. Also numerical results showed that the system with the H_2O–LiBr mixture has higher *COP* values but it can operate in a more narrow range of the generator temperatures compared to the systems using ammonia-based mixtures, because of its crystallization possibility. NH_3–$LiNO_3$ solution is more advantageous according to other solutions especially at low generator temperatures ($T_G < 75\ ^\circ C$).

The much higher improvement in *COP* was obtained by using the *SHE* compared to the *RHE* and *SRHE*. The maximum increase in *COP* was 66% by using the *SHE*, 14% and only 6% by using the *RHE* and *SRHE*, respectively. For that reason, the *SRHE* may not be considered practically significant.

It is hoped that many operations on absorption refrigeration cycles such as the selection of appropriate working solution pair with respect to operating conditions, the accurate and fast calculation of performance parameters, and the determination of suitable operating conditions could be done by the developed user-friendly software package. This study can be a useful source for researchers, since it includes a review of absorption refrigeration systems and a detailed thermodynamic analysis of the system including three heat exchangers, and comprehensive information related to conventional working fluids and alternatives.

References

[1] Riffat SB, Afonso CF, Oliveira AC, Reay DA. Natural refrigerants for refrigeration and air-conditioning systems. Appl Therm Eng 1997;17:33–42.
[2] Riffat SB, James SE, Wong CW. Experimental analysis of the absorption and desorption rates of $HCOOK/H_2O$ and $LiBr/H_2O$. Int J Energy Res 1998;22: 1099–103.
[3] Dincer I. Refrigeration systems and applications. John Wiley and Sons; 2003.
[4] Ajib S, Karno A. Thermo physical properties of acetone–zinc bromide for using in a low temperature driven absorption refrigeration machine. Heat Mass Transfer 2008;45:61–70.
[5] Karno A, Ajib S. Thermodynamic analysis of an absorption refrigeration machine with new working fluid for solar applications. Heat Mass Transfer 2008;45:71–81.
[6] Pilatowsky I, Rivera W, Romero RJ. Thermodynamic analysis of monomethylamine–water solutions in a single-stage solar absorption refrigeration cycle at low generator temperatures. Solar Energy Mater Solar Cells 2001;70:287–300.
[7] Pilatowsky I, Rivera W, Romero JR. Performance evaluation of a monomethylamine–water solar absorption refrigeration system for milk cooling purposes. Appl Therm Eng 2004;24:1103–15.
[8] Romero RJ, Guillen L, Pilatowsky I. Monomethylamine–water vapour absorption refrigeration system. Appl Therm Eng 2005;25:867–76.
[9] Mittal V, Kasana KS, Thakur NS. Performance evaluation of solar absorption cooling system of Bahal (Haryana). J Indian Inst Sci 2005;85:295–305.
[10] De Lucas A, Donate C, Villasenor J, Rodriguez JF. Performance evaluation and simulation of a new absorbent for an absorption refrigeration system. Int J Refrig 2004;27:324–30.
[11] De Lucas A, Donate M, Rodriguez JF. Applying surfactants to improve the absorption capacity of mixtures of lithium bromide and formates in absorption refrigeration coolers. Int J Refrig 2008;31(6):1073–80.
[12] Ferreira CAI. Thermodynamic and physical property data equations for ammonia–lithium nitrate and ammonia–sodium thiocyanate solutions. Solar Energy 1984;32:231–6.

[13] Sun DW. Comparison of the performance of NH_3–H_2O, NH_3–$LiNO_3$ and NH_3–NaSCN absorption refrigeration systems. Energy Convers 1998;39(5/6): 357–68.
[14] Abdulateef JM, Sopian K, Alghoul MA, Sulaiman MY, Zaharim A, Ahmad I. Solar absorption refrigeration system using new working fluid pairs. Int J Energy 2007;1(3):82–7.
[15] Zhu L, Gu J. Thermodynamic analysis of a novel thermal driven refrigeration system. World Acad Sci Eng Technol 2009;56:351–5.
[16] Safarov JT. The investigation of the (p, ρ, T) and (p_s, ρ_s, T_s) properties of $\{(1-x)CH_3OH + xLiBr\}$ for the application in absorption refrigeration machines and heat pumps. J Chem Thermodyn 2003;35:1929–37.
[17] Safarov JT. Study of thermodynamic properties of binary solutions of lithium bromide or lithium chloride with methanol. Fluid Phase Equilibr 2005;236: 87–95.
[18] Sencan A. Modeling of thermodynamic properties of refrigerant/absorbent couples using data mining process. Energy Convers Manage 2007;48:470–80.
[19] Muthu V, Saravanan R, Renganarayanan S. Experimental studies on R134a-DMAC hot water based vapour absorption refrigeration systems. Int J Therm Sci 2008;47:175–81.
[20] Kaita Y. Thermodynamic properties of lithium bromide–water solutions at high temperatures. Int J Refrig 2001;24:374–90.
[21] Chua HT, Toh HK, Malek A, Ng KC, Srinivasan K. Improved thermodynamic property field of LiBr–H_2O solution. Int J Refrig 2000;23:412–29.
[22] Wu S, Eames IW. Innovations in vapour-absorption cycles. Appl Energy 2000;66:251–66.
[23] Saravanan R, Maiya MP. Thermodynamic comparison of water-based working fluid combinations for a vapor absorption refrigeration system. Appl Therm Eng 1998;18(7):553–68.
[24] Mostafavi M, Agnew B. The impact of ambient temparature on lithium bromide–water absorption machine performance. Appl Therm Eng 1996;16:515–22.
[25] Mostafavi M, Agnew B. The effect of ambient temperature on the surface area of components of an air-cooled lithium bromide/water absorption unit. Appl Therm Eng 1996;16:515–22.
[26] Horuz I. A comparison between ammonia–water and water–lithium bromide solutions in vapor absorption refrigeration systems. Int Commun Heat Mass Transfer 1998;25(5):711–21.
[27] Bulgan AT. Use of low temperature energy sources in aqua-ammonia absorption refrigeration systems. Energy Convers Manage 1997;38(14):1431–8.
[28] Bulgan AT, Koc A, Ozturk NA. Investigation of thermodynamic properties of alternative fluid couples for absorption thermal systems. Energy Convers Manage 2000;41:1029–42.
[29] Joudi KA, Lafta AH. Simulation of a simple absorption refrigeration system. Energy Convers Manage 2001;42:1575–605.
[30] Aphornratana S, Sriveerakul T. Experimental studies of a single-effect absorption refrigerator using aqueous lithium–bromide: effect of operating condition to system performance. Exp Therm Fluid Sci 2007;32:658–69.
[31] Mehrabian MA, Shahbeik AE. Thermodynamic modelling of a single-effect LiBr–H_2O absorption refrigeration cycle. Proc Inst Mech Eng Part E J Process Mech Eng 2005;219:261–73.
[32] Srikhirin P, Aphornratana S, Chungpaibulpatana S. A review of absorption refrigeration technologies. Renew Sustain Energy Rev 2001;5:343–72.
[33] Zhai XQ, Wang RZ. A review for absorbtion and adsorbtion solar cooling systems in China. Renew Sustain Energy Rev 2009;13:1523–31.
[34] Fan Y, Luo L, Souyri B. Review of solar sorption refrigeration technologies: development and applications. Renew Sustain Energy Rev 2007;11:1758–75.
[35] Donate M, Rodriguez L, De Lucas A, Rodriguez JF. Thermodynamic evaluation of new absorbent mixtures of lithium bromide and organic salts for absorption refrigeration machines. Int J Refrig 2006;29:30–5.
[36] Sozen A, Ozalp M. Performance improvement of absorption refrigeration system using triple-pressure-level. Appl Therm Eng 2003;23:1577–93.
[37] Abu-Ein SQ, Fayyad SM, Momani W, Al-Bousoul M. Performance analysis of solar powered absorption refrigeration system. Heat Mass Trans 2009;46: 137–45.
[38] Kaynakli O, Kilic M. Theoretical study on the effect of operating conditions on performance of absorption refrigeration system. Energy Convers Manage 2007;48:599–607.
[39] Sencan A. Performance of ammonia–water refrigeration systems using artificial neural networks. Renew Energy 2007;32:314–28.
[40] Sozen A, Arcaklioglu E, Ozalp M. Formulation based on artificial neural network of thermodynamic properties of ozone friendly refrigerant/absorbent couples. Appl Therm Eng 2005;25:1808–20.
[41] Misra RD, Sahoo PK, Sahoo S, Gupta A. Thermoeconomic optimization of a single effect water/LiBr vapour absorption refrigeration system. Int J Refrig 2003;26:158–69.
[42] Asdrubali F, Grignaffini S. Experimental evaluation of the performances of a H_2O–LiBr absorption refrigerator under different service conditions. Int J Refrig 2005;28:489–97.
[43] Horuz I, Callander TMS. Experimental investigation of a vapor absorption refrigeration system. Int J Refrig 2004;27:10–6.
[44] Darwish NA, Al-Hashimi SH, Al-Mansoori AS. Performance analysis and evaluation of a commercial absorption–refrigeration water–ammonia (ARWA) system. Int J Refrig 2008;31:1214–23.
[45] Venegas M, Izquierdo M, de Vega M, Lecuona A. Thermodynamic study of multistage absorption cycles using low-temperature heat. Int J Energy Res 2002;26:775–91.
[46] Wang JF, Gao GC, Chen GM. An improved absorption refrigeration cycle driven by unsteady thermal sources below 100 °C. Int J Energy Res 2000;24:633–40.
[47] Zohar A, Jelinek M, Levy A, Borde I. Numerical investigation of a diffusion absorption refrigeration cycle. Int J Refrig 2005;28:515–25.
[48] Zohar A, Jelinek M, Levy A, Borde I. The influence of diffusion absorption refrigeration cycle configuration on the performance. Appl Therm Eng 2007;27:2213–9.
[49] Zohar A, Jelinek M, Levy A, Borde I. Performance of diffusion absorption refrigeration cycle with organic working fluids. Int J Refrig 2009;32:1241–6.
[50] Koyfman A, Jelinek M, Levy A, Borde I. An experimental investigation of bubble pump performance for diffusion absorption refrigeration system with organic working fluids. Appl Therm Eng 2003;23:1881–94.
[51] Fernandez-Seara J, Sieres J, Vazquez M. Compression–absorption cascade refrigeration system. Appl Therm Eng 2006;26:502–12.
[52] Zhao Y, Shigang Z, Haibe Z. Optimization study of combined refrigeration cycles driven by an engine. Appl Energy 2003;76:379–89.
[53] He Y, Chen G. Experimental study on an absorption refrigeration system at low temperatures. Int J Therm Sci 2007;46:294–9.
[54] He Y, Hong R, Chen G. Heat driven refrigeration cycle at low temperatures. Chin Sci Bull 2005;50:485–9.
[55] Manzela AA, Hanriot SM, Cabezas-Gomez L, Sodre JR. Using engine exhaust gas as energy source for an absorption refrigeration system. Appl Energy 2010;87:1141–8.
[56] Koehler J, Tegethoff WJ, Westphalen D, Sonnekalb M. Absorption refrigeration system for mobile applications utilizing exhaust gases. Heat Mass Transfer 1997;32:333–40.
[57] Hilali I, Soylemez MS. On the optimum sizing of exhaust gas-driven automotive absorption cooling systems. Int J Energy Res 2008;32:655–60.
[58] Sun ZG, Guo KH. Cooling performance and energy saving of a compression–absorption refrigeration system driven by a gas engine. Int J Energy Res 2006;30:1109–16.
[59] Arun MB, Maiya MP, Murthy SS. Equilibrium low pressure generator temperatures for double-effect series flow absorption refrigeration systems. Appl Therm Eng 2000;20:227–42.
[60] Wu S. Investigation of ejector re-compression absorption refrigeration cycle. University of Nottingham for the degree of Doctor of Philosophy; May 1999.
[61] Sozen A. Effect of heat exchangers on performance of absorption refrigeration systems. Energy Convers Manage 2001;42:1699–716.
[62] Romero RJ, Rivera W, Gracia J, Best R. Theoretical comparison of performance of absorption heat pump system for cooling and heating operating with an aqueous ternary hydroxide and water/lithium bromide. Appl Therm Eng 2001;21:1137–47.